Published in final edited form as:
Biochemistry. 2010 September 7; 49(35): 7674–7682. doi:10.1021/bi100973m.

Identification of a regulatory segment of poly(ADP-ribose) glycohydrolase†

Davide Botta and **Myron K. Jacobson***
Department of Pharmacology and Toxicology, College of Pharmacy and Arizona Cancer Center, University of Arizona, Tucson, AZ 85724, USA

Abstract

Coordinate regulation of PARPs-1/2 and PARG is required for cellular responses to genotoxic stress. While PARPs-1/2 are regulated by DNA breaks and covalent modifications, mechanisms of PARG regulation are poorly understood. We report here discovery of a PARG regulatory segment far removed linearly from residues involved in catalysis. Expression and analysis of human PARG segments identified a minimal catalytically active C-terminal PARG (hPARG59) containing a 16-residue N-terminal mitochondrial targeting sequence (MTS). Deletion analysis and site-directed mutagenesis revealed that the MTS, specifically hydrophobic residues L473 and L474 were required for PARG activity. This region of PARG was termed “Regulatory Segment/MTS” (REG/MTS). The overall α-helical composition of hPARG59, determined by circular dichroism (CD), was unaffected by mutation of the REG/MTS leucine residues, suggesting that activity loss was not due to incorrect protein folding. REG/MTS was predicted to be in a loop conformation since the CD spectra of mutant Δ1-16 lacking the REG/MTS showed a higher α-helical content compared to hPARG59, indicating a secondary structure other than α-helix for this segment. Deletion of the REG/MTS from full-length hPARG111 also resulted in complete loss of activity, indicating that all PARG isoforms are subject to regulation at this site. Presence of the REG/MTS raises the possibility that PARG activity is regulated by interactions of PARPs-1/2 and other proteins at this site, raises interesting questions concerning mitochondrial PARG since MTS residues are often removed after transport, and offers a potentially novel site for drug targeting of PARG.

The synthesis of polymers of ADP-ribose (PAR)1 is an immediate cellular response to DNA strand breaks caused by oxidative stress, ionizing radiation or alkylating agents (1–3). A primary enzyme involved in this post-translational modification is poly (ADP-ribose) polymerase-1 (PARP-1), which belongs to a growing family of PARPs that includes a second member (PARP-2) that also responds to DNA strand breaks (4,5). Upon binding to DNA strand breaks, PARPs-1/2 use nicotinamide adenine dinucleotide (NAD^+) as a substrate to synthesize PAR targeted to the PARPs themselves and other nuclear acceptor proteins, such as histones, p53 and enzymes involved in DNA repair (6). PARP-1 is inactivated and released from the DNA strand break by its automodification. Poly(ADP-

†Supported by research grant CA 43894 from the National Institutes of Health to M.K.J.

To whom correspondence should be addressed: Arizona Cancer Center Room 3985, University of Arizona, 1515 North Campbell Avenue, Tucson, AZ 85724, USA. Tel: (520) 626-5957. Fax: (520) 626-8657. mjacobson@pharmacy.arizona.edu.

[1]**Abbreviations:** ADP, adenosine-5′-diphosphate; PAR, poly(ADP-ribose); PARG, poly(ADP-ribose) glycohydrolase; hPARG, human PARG; PARP-1/2, poly(ADP-ribose) polymerase 1 and 2; ADPR, ADP-ribose; ADPRT, ADP-ribosyltransferase; NAD^+, nicotinamide adenine dinucleotide; MTS, mitochondrial targeting sequence; CD, circular dichroism; MEF, mouse embryonic fibroblasts; XRCC1, x-ray repair cross complementing group 1; ERK1/2, extracellularly regulated kinases 1 and 2; PCR, polymerase chain reaction; TEV, tobacco etch virus; PMSF, phenylmethylsulfonyl fluoride; Ni-NTA, nickel-nitrilotriacetic acid; MBP, maltose binding protein; BSA, bovine serum albumin; TLC, thin layer chromatography; SDS, sodium dodecyl sulfate; MPP, mitochondrial processing peptidase; SSL, synthetic sickness/lethality.

ribose) glycohydrolase (PARG) is the endo-exoglycohydrolase that catalyzes PAR turnover via the hydrolysis of the α(1″ → 2′) and α(1‴ → 2″) ribosyl-ribose linkages to produce free ADP-ribose (ADPR) (7).

Unlike the PARPs that are encoded by multiple genes, only a single PARG gene with a clearly defined function in PAR hydrolysis has been detected in mammals (8). A structurally unrelated 39-kDa enzyme exhibiting PARG activity has been identified and characterized (9), but its functional significance remains to be elucidated. The PARG gene encodes a full-length 111-kDa PARG protein (hPARG111) that localizes to the nucleus, but several other PARG isoforms are expressed in different cell compartments from alternative splice variants of the human *PARG* RNA transcripts (10,11). These include hPARG102 and hPARG99, which lack the N-terminal nuclear localization signal (NLS) coded by exon 1 and show an extranuclear localization (10), and a hPARG59 isoform that localizes to the mitochondria (11,12).

Several significant strides in understanding the structural and functional relationship of PARG have been made in the last decade. Deletion of the PARG gene results in a complete loss of cellular PARG activity and early embryonic lethality of homozygous mutant mice (13) suggesting that there are no significant compensatory mechanisms for the catabolism of PAR. Partial deletion of the PARG gene in both *Drosophila melanogaster* (14) and in mice (13,15) sensitizes cells to DNA damage induced by alkylating agents and ionizing radiation. Upon genotoxic stress, both PARP-$1^{-/-}$ mouse embryonic fibroblasts (MEF) (16) and cells derived from a hypomorphic mutant mouse model in which exons 2 and 3 of PARG were deleted (PARG-Δ2,3) (17) showed a reduced formation of XRCC1 foci, indicating that the regulation of PAR levels is achieved via a precise coordination of PARP and PARG activities critical for normal cellular responses to DNA damage.

An inhibitor binding site of PARG, T796, was recently identified (18) and found to be in a highly conserved region of the protein coded by exons 13 and 14, which also contains three catalytically essential acidic residues, namely D738, E756 and E757 (19) and a glycine-rich region G745-G746-G747 (20) important for PARG function. These findings allowed for a ‘signature sequence’ to be defined and led to the putative assignment of a domain structure for PARG (Figure 1) (19,21).

Extensive work on PARP-1 has led to the discovery of several different mechanisms of regulation for this enzyme. Two N-terminal zinc finger domains in PARP-1 have been shown to bind to various DNA structures (22) and thereby activate the catalytic domain situated at the C-termini of the enzymes. Recently, a third zinc-binding domain has been identified in human PARP-1, and it has been shown to be essential for the DNA-dependent activity (23) as well as the chromatin compaction activity of the enzyme (24). Both PARP-1 activation following DNA damage (25) and DNA damage-independent PARP-1 activation (26) was found to be dependent on phosphorylation by activated extracellular signal-regulated kinases 1/2 (ERK1/2) (25) and the role of PARP-1 in transcriptional regulation was found to be regulated by acetylation of specific lysine residues (27). In spite of our increasing understanding of PARP-1 regulation, to date no information is available on how PARG is regulated. We report here structure/function studies that have led to the discovery of the first potential mechanism of regulation of PARG via the identification of amino acid residues required for PARG activity that are far removed from the putative catalytic domain of the enzyme. Intriguingly, these residues are located within a 16-residue mitochondrial targeting sequence (MTS) of the enzyme.

MATERIALS AND METHODS

Materials

The pMAL-c2x and pBAD102/D-TOPO parent vectors were purchased from New England Biolabs (Ipswich, MA) and Invitrogen (Carlsbad, CA), respectively. The [α-^{32}P]-NAD^{+} used for the synthesis of radiolabeled PAR was purchased from Perkin Elmer (Waltham, MA).

Synthesis and cloning of PARG fragments and mutants

Primers were designed so as to produce Polymerase Chain Reaction (PCR) products with the ENLYFQ/S Tobacco Etch Virus (TEV) protease cleavage site coding sequence preceding each PARG fragment and mutant, and with SalI and PmeI restriction sites at the 5′ and 3′ ends, respectively. The PARG mutants were synthesized with the use of previously constructed and reported mutant PARG plasmids as templates for the PCR reaction (12). Each PCR product was cloned into a dual hexahistidine-maltose binding protein (His_6-MBP) fusion protein expression vector pMAL-His_6-malE, a modified pMAL-c2x expression vector (New England Biolabs) in which hexahistidine coding bases were inserted at the 5′ end of the malE gene that codes for the MBP tag (Figure 2A). Plasmids were amplified in electrocompetent *E. coli* TOP10 (Invitrogen), isolated using the QIAprep Spin Miniprep kit (Qiagen) and sequenced to ensure correct orientation of the PARG inserts.

Deletion mutations of the MTS

The QuikChange® II XL Site-Directed Mutagenesis Kit (Stratagene) was used, following the manufacturer's protocol, to obtain a deletion mutation of residues 461–476 in the full-length hPARG111 protein. Briefly, pBAD102/D-TOPO-hPARG111, a large expression vector containing the full-length protein, was amplified in its entirety by PCR using the PfuUltra™ High-Fidelity DNA polymerase and deletion primers hP111-Δ461-476for (5′-GGC TTG GAA CTC CCA TTG AGG AGT CTG CCA ATC ACA CAG TAA CTA TTC GG-3′) and hP111-Δ461-476rev (5′-CCG AAT AGT TAC TGT GTG ATT GGC AGA CTC CTC AAT GGG AGT TCC AAG CC-3′). The amplification reaction product was treated with the restriction enzyme *DpnI* for the digestion of parental methylated and hemimethylated DNA, and then transformed into XL10-Gold ultracompetent cells for amplification.

Expression and purification of PARG fragments and mutants

The pMAL-His_6-malE-TEV-hPARG plasmids were transformed into electrocompetent *E. coli* K12 TB1 strain (New England Biolabs) by electroporation. Cells were grown in 500 ml Rich media (10 g/L bacto-tryptone, 5 g/L yeast extract, 5 g/L NaCl and 2 g/L D-glucose) containing 100 μg/ml ampicillin until the A_{600} reached 0.5–0.6. Expression was induced by the addition of IPTG to a final concentration of 0.3mM. Cells were then grown for an additional 2 hours at 37°C, harvested by centrifugation and stored at −80°C. The pBAD102/D-TOPO-hPARG plasmids were instead transformed into electrocompetent *E. coli* Rosetta strain (Novagen), grown in LB media and expressed for 4 hours using 0.2% L-arabinose. Thawed cells were resuspended in lysis buffer (50 mM potassium phosphate buffer, pH 7.5, 300mM KCl, 50 mM imidazole, 10% glycerol, 0.1% triton X-100, 1 mM PMSF, 1 mg/ml aprotonin, 1 mg/ml leupeptin and 1 mg/ml pepstatin A) and subjected to sonificstion to rupture the cell membrane. After a 30 min centrifugation at 10000 rpm, the supernatant was loaded onto a 0.5-ml Ni-NTA agarose column (Invitrogen) and allowed to pass through by gravity flow. The column was washed twice with 5 ml of wash buffer (similar to the lysis buffer but lacking the protease inhibitors), and the protein was eluted with 1.5ml of elution buffer (50mM potassium phosphate buffer, pH 7.5, 300 mM KCl, 100 mM imidazole, 10%

glycerol, 0.1% triton X-100 and 1mM maltose). Following addition of 40 units of HQ-tagged TEV (Promega) to 40 μg of purified protein (1U: 1μg), the cleavage reaction was carried out in the elution buffer for 16 hours at 4°C.

PARG activity assay

This assay utilizes conditions previously reported (28). Briefly, a typical reaction mixture was prepared by adding 5 μl of 3x glyco assay buffer (150 mM potassium phosphate buffer, pH 7.5, 150 mM KCl, 0.3 mg/ml BSA and 30 mM 2-mercaptoethanol), 2.5 μl of 60 μM [α-^{32}P]-PAR (approx. 6000 cpm/μl) and 5 μl of deionized water. A total of 2.5 μl of each TEV-cleavage reaction product was added and the reaction mixtures were incubated at 37°C for 10–60 minutes. The reactions were then stopped by the addition of 2 μl of 1% SDS. Next, 3 μl of each reaction mixture was loaded onto a 2 × 10 cm poly(ethyleneimine)-cellulose F TLC plate, prespotted with 1 μl of 40 mM ADP-ribose. The spots were dried and the plates were placed into a TLC tank with 100 ml of methanol and developed until the solvent front reached the top of the plate. The plates were then transferred into a second tank containing 100 ml of a 0.9 M/0.3 M acetic acid/LiCl solution. Once developed, the plates were air-dried, and the origins (containing PAR) and ADPR spots (visible under a short-wave UV lamp) were excised and placed into separate 20-ml scintillation vials containing 10 ml EcoLume. The radioactivity was counted in a Beckman liquid scintillation counter.

Circular Dichroism (CD) Spectrophotometry

CD spectra were recorded in the wavelength range 200–260 nm with an Olis DSM20 spectropolarimeter (Jasco, Easton, MD) using a 0.1-cm path length stain-free cell. The fusion proteins were analyzed at a concentration of 0.3 mg/ml in 5mM KH_2PO_4, pH 7.5, 25 mM KCl and 1% glycerol at 20°C. Spectra were recorded in millidegrees of ellipticity (θ). The solvent spectrum was subtracted from the sample spectra, and three independent measurements were used to calculate the mean residue ellipticity, $[\theta]$, using the formula:

$$[\theta]=(100\theta)\div(clN)$$

where $[\theta]$ is the mean residue ellipticity in degrees squared centimeters per decimole (deg cm^2 dmol^{-1}), θ is the experimental ellipticity in millidegrees, c is the protein concentration in millimolarity, l is the cell path length in centimeters, and N is the number of residues in the protein (29). Assuming that the mean residue ellipticity at 222 nm is exclusively due to the α-helix conformation, fractional helicities were calculated using the following equation:

$$\%\ helicity=(([\theta]_{222\ nm}+2,340\ deg\ cm^2 dmol^{-1})\div 30,300\ deg\ cm^2 dmol^{-1})\times 100$$

where $[\theta]_{222\ nm}$ is the observed mean residue ellipticity at 222 nm, and 2,340 deg cm^2 dmol^{-1} and 30,300 deg cm^2 dmol^{-1} are previously determined values corresponding to 0 and 100% helix content at 222 nm, respectively (30).

Secondary structure predictions

The secondary structures of PARP-1, PARP-2 and PARG were predicted by submitting primary sequences to the online PredictProtein server (31). The reported results were obtained with the PHD (EMBL-Heidelberg) (32) and PROF$_{sec}$ (Profile network prediction Heidelberg) (33) algorithms. PROF$_{sec}$ is currently one of the most reliable profile-based neuronal network systems for predicting secondary structures of proteins with a three-state per-residue accuracy of 76 percent (34). MTS predictions were made using the MitoProtII computational method (35).

RESULTS

The minimal catalytically active PARG is a 59-kDa C-terminal fragment

Previous work by our laboratory identified a highly conserved inhibitor-binding residue of PARG, T796 (18), as well as three essential catalytic residues, D738, E756 and E757 (19), all localized in a region of the putative domain C coded by exons 12 and 13 of the human PARG gene. These findings, together with the functional characterization of a glycine-rich segment, G745-G746-G747 (20), also present in this region of PARG, allowed for the definition of a 'PARG signature' sequence that suggested that the putative domain C represented the minimal catalytic domain of PARG. In order to test this hypothesis, 15 different fragments of human PARG cDNA were cloned into a His_6-MBP fusion protein expression vector as described in Materials and Methods. Each PARG fragment was expressed, purified by affinity chromatography, cleaved using TEV protease and tested for PARG activity. The PARG assay used in this study measures the release of free ADP-ribose, thus measuring the exoglycosidase activity of PARG, which represents the major activity of the enzyme. Analysis of each PARG fragment was made by SDS-PAGE and Coomassie Blue Staining to confirm expression, purity and TEV cleavage efficiency prior to catalytic activity determination. Figure 2B shows the high degree of purity (lane 1) and efficient TEV cleavage (lane 2) of hPARG59, one of the larger fragments tested, as an example of the purity verification. Michaelis-Menten kinetic analyses performed on hPARG59 showed that the K_m and V_{max} values for this fragment prior to and after removal of the His_6-MBP tag were similar (Figure 2C) indicating that the 45-kDa His_6-MBP dual tag did not exert a significant effect on PARG activity. For these experiments, activity of both cleaved and uncleaved proteins was examined. The fragments were designed so as to include the active site residues coded by exons 12 and 13 and vary in the number of exon-coded residues included on either side of the active site region (Figure 1). The designation of each fragment corresponds to its size in kilodaltons. Unexpectedly, only the largest two fragments, hPARG70 and hPARG59, demonstrated enzymatic activity. Similar results were observed with the corresponding uncleaved fusion proteins (data not shown).

The results in Figure 1 identified hPARG59 as the minimal catalytically active protein among the fragments analyzed. We were particularly intrigued by the lack of enzymatic activity of hPARG56, a fragment that differs from the active hPARG59 only by its lack of twenty-six residues coded by exon 4, which contain a recently detected 16-residue N-terminal MTS (11,12).

Deletion of the PARG MTS results in the complete loss of catalytic activity

To assess the role of the 16-residue MTS in the catalytic activity of PARG, 4 different deletion mutants were constructed (Figure 3). Each mutant was expressed, purified, cleaved with TEV, and tested for activity as described in Materials and Methods. The specific activity of each protein was measured using results from two separate experiments, each analyzed in triplicate assays. The activity of the deletion mutants was compared to that of the active minimal catalytic fragment, hPARG59, which possesses the full MTS. The deletion of the first four residues of the MTS, namely M1, R2, R3 and M4 (mutant Δ1-4) resulted in approximately a 70 percent decrease in catalytic activity compared to hPARG59. As the deletion progressed towards the C-terminal end of the MTS, the activity decreased to a minimum where the deletion of residues M1 to P12 (mutant Δ1-12) as well as the entire MTS (mutant Δ1-16) resulted in no detectable activity. These results indicate that the amino acids present in the MTS of PARG are required for the activity of the enzyme.

Adjacent hydrophobic residues L13 and L14 in the C-terminal half of the MTS are essential for PARG function

A general feature of many MTS is an amphipathic alpha helix (11,36). Despite a lack of primary sequence homology, MTS are generally highly basic, contain no acidic residues and have a high percentage of leucine, serine and arginine residues. In order to determine which residues are essential for PARG activity, the MTS was interrogated by site-directed mutagenesis. The basic arginine residues at positions 2, 3, 6 and 10 were mutated to hydrophobic alanine residues to reduce the net positive charge of the MTS, and the hydrophobic leucine residues at positions 11, 13 and 14 were mutated to acidic aspartate residues to disturb the hydrophobic region of the MTS while retaining similar side-chain size. Figure 3 shows the mutants constructed and the effect on PARG activity. The R2A mutation alone was the only arginine mutation to result in a significant loss of PARG activity, which was circa 50 percent of that of wild-type hPARG59. The R3A and the combined R2A/R3A/R6A/R10A mutations had no significant effect on PARG activity, while the R6A and R10A mutations resulted in a significant increase in activity. The L11D mutation alone did not decrease PARG activity. However, the double L11D/L13D mutant almost entirely abolished it, and the triple L11D/L13D/L14D mutant resulted in no detectable activity. These findings complement the deletion mutation results by identifying a regulatory segment in the MTS region of PARG. Specifically, they point to the vicinal hydrophobic residues L13 and L14 as residues crucial for PARG activity. We have termed this region of PARG “Regulatory Segment/MTS” (REG/MTS).

Loss of PARG activity is not due to incorrect protein folding

CD spectroscopy was performed to determine whether the differences in catalytic activity between hPARG59 and inactive fragments and mutants was due to protein unfolding. Inactive constructs chosen for CD analysis were hPARG42 (consisting of domains C and D), hPARG23 (consisting of domain C only), Δ1-16 (lacking the REG/MTS), and mutant L11D/L13D/L14D. Comparisons of the CD spectra and the mean residue ellipticity values at 222 nm are shown in Figure 4A and 4B, respectively. The hPARG59 displayed a double minima at 208 and 222 nm consistent with those observed for canonical α-helices. Any protein unfolding, therefore, would be expected to increase the amount of random coil present in the population, and the minima at 222 and 208 nm on the CD spectra would become shallower and move to lower wavelengths, respectively. The deletion of Domain B from hPARG59 (fragment hPARG42) resulted in a 2 percent decrease in helicity. However, the overall molecular population remained mostly α-helical. Domain C alone (hPARG23), on the other hand, showed a much larger decrease in helical content of circa 10 percent and the spectrum showed a greater overall β-sheet content as supported by a weaker CD signal, the formation of a single minima in the 210–220 nm region and a significant lowering of the maxima at 200 nm. Surprisingly, the deletion of the REG/MTS (Δ1-16) resulted in an increase in helicity. This was unexpected due to the α-helical nature of most MTS (36, 37) and suggests a different secondary structure for this sequence in PARG. Lastly, the mutation of the three hydrophobic leucine residues of the REG/MTS (mutant L11D/L13D/L14D) caused no detectable changes in the confirmation of the protein. In addition to excluding loss of secondary structure as the cause of loss of enzymatic activity by deletion or mutation of the REG/MTS, these results provide an insight into the molecular composition of the different PARG domains, whose structures still remain to be determined.

Prediction of hPARG59 secondary structure

Due to the lack of a crystal structure of PARG, current knowledge on the molecular folding of the different putative PARG domains is limited. To complement the CD data obtained, secondary structure predictions were made using the PHD and $PROF_{sec}$ algorithms as described in Materials and Methods. Figure 5 shows the prediction models for human

PARP-1 (amino acids 664-1014), human PARP-2 (amino acids 233-583), and hPARG59 (amino acids 461-976). The corresponding crystal structures of human PARP-1 and PARP-2 (Protein Data Bank Identification numbers 2RCW and 3KJD, respectively) were included to validate the accuracy of the prediction algorithm. The prediction of PARP-1 and PARP-2 secondary structures very closely matches their crystal structures, with a mostly α-helical N-terminal domain followed by a mixed α/β catalytic ADP-ribosyltransferase (ADPRT) domain. β-sheet 5 (labeled by a red square) in the ADPRT domain contains the catalytic E988 and E534 residues of PARP-1 and PARP-2, respectively. These similarities highlight the potential for these algorithms to relate secondary structure predictions to functional aspects. The catalytic domain C of PARG predicts a very similar secondary structure to the PARP-1 and PARP-2 ADPRT domains, which contains a mixture of six β-sheets and three α-helices, and with the localization of the catalytic E756 and E757 residues in β-sheet 5 as seen for PARP-1 and PARP-2. The high incidence of β-sheets in the catalytic domain of PARG emphasizes their major catalytic role in PAR catabolism. Furthermore, Domain D is predicted to contain a mostly α-helical region similar to the domains on the N-terminal side of the PARP-1 and PARP-2 ADPRT domains. Hence, based on these secondary structure predictions, the ADPRT-like Domain C and the mostly α-helical Domain D of PARG highly resemble those of PARP-1 and PARP-2, with the sole difference being their relative orientation. Such findings can be rationalized by the similarity shared between the substrates of the two classes of enzymes, namely the ADPR moiety.

Domain B of PARG, on the other hand, is predicted to contain a mixture of random coils, α-helices and β-sheets. The N-terminus region that includes the REG/MTS is predicted to contain random coils followed by two vicinal β-sheets and four consecutive C-terminal α-helices. A more detailed analysis of the REG/MTS was carried out using the Sub_{sec} algorithm, a subset of $PROF_{sec}$ that predicts the secondary structure of residues that exhibit an average accuracy greater than 82 percent (Figure 6A). The REG/MTS was predicted to be in a loop conformation, which was not affected by the L11D/L13D/L14D mutations. The high probability of hPARG59 to be imported into the mitochondria, as predicted by the MitoProtII computational method (35), however, was greatly reduced by the L11D/L13D/L14D mutations (Figure 6B). In addition, the mutations prevented the detection of a mitochondrial processing peptidase (MPP) cleavage site. These predictions are in agreement with previously reported results showing a 75 percent reduction in mitochondrial import of the mutant compared to wild-type hPARG59 (12). The disruption of hydrophobicity of the REG/MTS, therefore, not only affects mitochondrial localization of hPARG59 but also its enzymatic activity. However, this loss of activity is not accompanied by any large change in secondary structure.

The REG/MTS is also a critical factor in the catalytic activity of full-length hPARG111

The role of the newly identified regulatory segment in the hPARG59 mitochondrial isoform was investigated in the full-length nuclear hPARG111 protein to determine whether this region could also regulate the enzymatic activity of larger PARG isoforms. While in hPARG59 the regulatory segment corresponds to the N-terminal MTS, in hPARG111 it is an internal region composed of amino acids 461-476 (Figure 1). The REG/MTS was deleted from hPARG111 by site-directed mutagenesis as described in Materials and Methods. As expected, hPARG111 was found to be active, with a specific activity comparable to that of hPARG59 (Figure 7). The hPARG111Δ461-476 deletion mutant, however, exhibited no detectable enzymatic activity, indicating that hPARG111, and consequently also the extranuclear hPARG102 and hPARG99 isoforms, also possess this mechanism of regulation.

DISCUSSION

The study presented here was initiated to identify the minimal catalytic domain of PARG. The identification of an inhibitor-binding site (18), three essential catalytic residues (19) and a functional glycine-rich region (20) all within the putative Domain C of PARG pointed to this highly conserved region as the putative minimal catalytic domain. Surprisingly, the smallest active fragment was found to be a 59-kDa fragment, also recently identified as a PARG mitochondrial isoform with an N-terminal MTS required for targeting to the mitochondrial matrix (11,12). Deletion studies and site-directed mutagenesis of the 16-residue MTS have identified this region, in particular the vicinal hydrophobic leucine residues L13 and L14, as required for PARG activity (Figure 3) revealing that the residues within the MTS are involved in the regulation of PARG.

The deletion of the REG/MTS from hPARG59 led to an increase in α-helical content of the protein, which was surprising since the positively-charged, amphipathic MTS segments of many proteins are typically predicted to form an α-helix (11). In contrast, secondary structure analyses in the study reported here using the $PROF_{sec}$ and SUB_{sec} algorithms predicted the REG/MTS to be in a loop conformation (Figure 6A). This prediction is in agreement with the CD data (Figure 4) since the deletion of this loop would be predicted to lower the random coil contribution to the spectrum and increase the α-helical fraction of the protein. Furthermore, a loop conformation would explain the lack of a detectable secondary structure change induced by the L11D/L13D/L14D mutation in the C-terminal hydrophobic half of the MTS. While amphiphilic properties are not limited to proteins having an α-helical MTS, and considerable flexibility exists in the structural requirements for MTS (38), another possibility could be that the formation of an α-helical structure is a downstream event induced by the interaction of hPARG59 with the binding site/cleft of its respective mitochondrial import receptor.

Our data supports a model whereby the hydrophobic leucine residues of the REG/MTS interact with hydrophobic residues near the catalytic site to activate PARG. Such a model is likely to apply to larger PARG isoforms across different cell compartments, since the deletion of the REG/MTS from the full-length hPARG111 also abrogated its catalytic activity. Indeed, the REG/MTS segment is present in all other isoforms of PARG that have been detected to date (10,11). This raises the possibility that as interactions of the REG/MTS with other proteins may generally be involved in PARG regulation. The interplay of PARP-1 and PARG in nuclear PAR metabolism makes automodified PARP-1 a likely candidate for regulation of PARG activity following DNA damage at the REG/MTS site.

The presence of a regulatory segment within the PARG MTS is particularly interesting in that the mechanism of mitochondrial import of proteins with an N-terminal MTS involves typically involves MTS cleavage by a MPP either during or after entry into the mitochondria (39,40). This fate of mitochondrial PARG is supported by the detection of an MPP cleavage site by the MitoProtII computational method (Figure 6B). This raises the possibility that interaction with other proteins would be required for activity of mitochondrial PARG. Recent studies have provided evidence for a mitochondrial localization of PARP-1, dependent on the presence of the mitochondrial protein Mitofilin, with which it interacts and which is poly(ADP-ribosyl)ated upon over-activation of PARP-1 by traumatic brain injury (41), although the presence of PARP-1 in the mitochondrial compartment has not yet been validated in cells derived from PARP-1 deficient animals.

While the mechanism of PARG regulation via this segment of PARG needs further investigation, it should be noted that a regulatory domain of PARP-1 involved in protein-protein interactions capable of modulating PARP-1 activation and crucial for its DNA-

dependent stimulation has recently been identified (23). This domain was found to contain four highly conserved cysteine residues with spacing reminiscent of the zinc finger protein fold, and was hence characterized as the third zinc-binding domain of PARP-1. Although the PARG regulatory segment only contains a single cysteine residue and does not have any detectable zinc-binding recognition signatures, it shares the same ability as PARP-1 in regulating catalytic activity from a location very distant from the active site (>250 residues). A comparison of six PARG sequences across a wide range of organisms revealed a high level of homology in the REG/MTS (Figure 8). Particular attention was given to the level of conservation of basic and hydrophobic residues, which was found to be high. Indeed, L14 is invariant across these organisms. The strong sequence homology provides further support for the notion that this region of PARG is involved in the regulation of PARG activity.

A look at the secondary structure predictions of hPARG59, in concert with the CD data, provides evidence for a mixed α/β Domain C and a mostly α-helical Domain D, which are very similar to the catalytic ADPRT domain and the mostly α-helical domain, respectively, of PARP-1 and PARP-2. The only significant difference lies in the orientation of the two domains. These predicted structural similarities between the active sites are due to the similar composition of their substrates, namely the ADPR moiety, and are further supported by the cross inhibition of PARG inhibitors with PARP-1 observed with several PARG inhibitors currently being developed in our laboratory (unpublished data). While this potential for cross inhibition may prove to have therapeutic benefits, particularly in the new paradigm of cancer therapy based on synthetic sickness/lethality (SSL), which has paved the way for the clinical development of PARP inhibitors in breast tumors with germline mutations in BRCA1 and/or BRCA2 (42,43), it also poses difficulties in obtaining specific PARG inhibitors. This newly identified regulatory segment of PARG, therefore, offers a potentially novel site for drug targeting which could be exploited for the development of specific and potent PARG inhibitors to serve as tools in the validation of PARG as a therapeutic target.

Acknowledgments

DNA sequence analyses were performed by the University of Arizona Genetic Analysis and Technology Core Service Facility. All circular dichroism experiments were performed at the University of Arizona Analytical Biophysics Core Facility run by Dr. Chad K. Park.

References

1. Juarez-Salinas H, Sims JL, Jacobson MK. Poly(ADP-ribose) levels in carcinogen-treated cells. Nature. 1979; 282:740–741. [PubMed: 229416]
2. Schreiber V, Dantzer F, Ame JC, de Murcia G. Poly(ADP-ribose): novel functions for an old molecule. Nat Rev Mol Cell Biol. 2006; 7:517–528. [PubMed: 16829982]
3. Heeres JT, Hergenrother PJ. Poly(ADP-ribose) makes a date with death. Curr Opin Chem Biol. 2007; 11:644–653. [PubMed: 17936669]
4. Kleine H, Poreba E, Lesniewicz K, Hassa PO, Hottiger MO, Litchfield DW, Shilton BH, Luscher B. Substrate-assisted catalysis by PARP10 limits its activity to mono-ADP-ribosylation. Mol Cell. 2008; 32:57–69. [PubMed: 18851833]
5. Hottiger MO, Hassa PO, Luscher B, Schuler H, Koch-Nolte F. Toward a unified nomenclature for mammalian ADP-ribosyltransferases. Trends Biochem Sci. 2010; 35:208–219. [PubMed: 20106667]
6. Lindahl T, Satoh MS, Poirier GG, Klungland A. Post-translational modification of poly(ADP-ribose) polymerase induced by DNA strand breaks. Trends Biochem Sci. 1995; 20:405–411. [PubMed: 8533153]

7. Miwa M, Tanaka M, Matsushima T, Sugimura T. Purification and properties of glycohydrolase from calf thymus splitting ribose-ribose linkages of poly(adenosine diphosphate ribose). J Biol Chem. 1974; 249:3475–3482. [PubMed: 4831224]
8. Lin W, Ame JC, Aboul-Ela N, Jacobson EL, Jacobson MK. Isolation and characterization of the cDNA encoding bovine poly(ADP-ribose) glycohydrolase. J Biol Chem. 1997; 272:11895–11901. [PubMed: 9115250]
9. Oka S, Kato J, Moss J. Identification and characterization of a mammalian 39-kDa poly(ADP-ribose) glycohydrolase. J Biol Chem. 2006; 281:705–713. [PubMed: 16278211]
10. Meyer-Ficca ML, Meyer RG, Coyle DL, Jacobson EL, Jacobson MK. Human poly(ADP-ribose) glycohydrolase is expressed in alternative splice variants yielding isoforms that localize to different cell compartments. Exp Cell Res. 2004; 297:521–532. [PubMed: 15212953]
11. Meyer RG, Meyer-Ficca ML, Whatcott CJ, Jacobson EL, Jacobson MK. Two small enzyme isoforms mediate mammalian mitochondrial poly(ADP-ribose) glycohydrolase (PARG) activity. Exp Cell Res. 2007; 313:2920–2936. [PubMed: 17509564]
12. Whatcott CJ, Meyer-Ficca ML, Meyer RG, Jacobson MK. A specific isoform of poly(ADP-ribose) glycohydrolase is targeted to the mitochondrial matrix by a N-terminal mitochondrial targeting sequence. Exp Cell Res. 2009; 315:3477–3485. [PubMed: 19389396]
13. Koh DW, Lawler AM, Poitras MF, Sasaki M, Wattler S, Nehls MC, Stoger T, Poirier GG, Dawson VL, Dawson TM. Failure to degrade poly(ADP-ribose) causes increased sensitivity to cytotoxicity and early embryonic lethality. Proc Natl Acad Sci U S A. 2004; 101:17699–17704. [PubMed: 15591342]
14. Hanai S, Kanai M, Ohashi S, Okamoto K, Yamada M, Takahashi H, Miwa M. Loss of poly(ADP-ribose) glycohydrolase causes progressive neurodegeneration in Drosophila melanogaster. Proc Natl Acad Sci U S A. 2004; 101:82–86. [PubMed: 14676324]
15. Cortes U, Tong WM, Coyle DL, Meyer-Ficca ML, Meyer RG, Petrilli V, Herceg Z, Jacobson EL, Jacobson MK, Wang ZQ. Depletion of the 110-kilodalton isoform of poly(ADP-ribose) glycohydrolase increases sensitivity to genotoxic and endotoxic stress in mice. Mol Cell Biol. 2004; 24:7163–7178. [PubMed: 15282315]
16. El-Khamisy SF, Masutani M, Suzuki H, Caldecott KW. A requirement for PARP-1 for the assembly or stability of XRCC1 nuclear foci at sites of oxidative DNA damage. Nucleic Acids Res. 2003; 31:5526–5533. [PubMed: 14500814]
17. Gao H, Coyle DL, Meyer-Ficca ML, Meyer RG, Jacobson EL, Wang ZQ, Jacobson MK. Altered poly(ADP-ribose) metabolism impairs cellular responses to genotoxic stress in a hypomorphic mutant of poly(ADP-ribose) glycohydrolase. Exp Cell Res. 2007; 313:984–996. [PubMed: 17276427]
18. Koh DW, Patel CN, Ramsinghani S, Slama JT, Oliveira MA, Jacobson MK. Identification of an inhibitor binding site of poly(ADP-ribose) glycohydrolase. Biochemistry. 2003; 42:4855–4863. [PubMed: 12718526]
19. Patel CN, Koh DW, Jacobson MK, Oliveira MA. Identification of three critical acidic residues of poly(ADP-ribose) glycohydrolase involved in catalysis: determining the PARG catalytic domain. Biochem J. 2005; 388:493–500. [PubMed: 15658938]
20. Panda S, Poirier GG, Kay SA. tej defines a role for poly(ADP-ribosyl)ation in establishing period length of the arabidopsis circadian oscillator. Dev Cell. 2002; 3:51–61. [PubMed: 12110167]
21. Oliveira MA, Koh DW, Patel CN, Jacobson MK. Structure-based characterization of a novel anticancer target poly(ADP-ribose) glycohydrolase (PARG): Evidence for the presence of an ADP-ribosyltransferase (ADPRT) fold. Proc Am Assoc Cancer Res. 2001; 42:832.
22. Rolli, V.; Ruf, A.; Augustin, A.; Schulz, GE.; Ménissier-de Murcia, J.; de Murcia, G. From DNA Damage and Stree Signaling to Cell Death: Poly ADP-ribosylation Reactions. de Murcia, G.; Shall, S., editors. Oxford University Press; New York: 2000.
23. Langelier MF, Servent KM, Rogers EE, Pascal JM. A third zinc-binding domain of human poly(ADP-ribose) polymerase-1 coordinates DNA-dependent enzyme activation. J Biol Chem. 2008; 283:4105–4114. [PubMed: 18055453]

24. Langelier MF, Ruhl DD, Planck JL, Kraus WL, Pascal JM. The Zn3 domain of human poly(ADP-ribose) polymerase-1 (PARP-1) functions in both DNA-dependent poly(ADP-ribose) synthesis activity and chromatin compaction. J Biol Chem. (in press).
25. Kauppinen TM, Chan WY, Suh SW, Wiggins AK, Huang EJ, Swanson RA. Direct phosphorylation and regulation of poly(ADP-ribose) polymerase-1 by extracellular signal-regulated kinases 1/2. Proc Natl Acad Sci U S A. 2006; 103:7136–7141. [PubMed: 16627622]
26. Cohen-Armon M, Visochek L, Rozensal D, Kalal A, Geistrikh I, Klein R, Bendetz-Nezer S, Yao Z, Seger R. DNA-independent PARP-1 activation by phosphorylated ERK2 increases Elk1 activity: a link to histone acetylation. Mol Cell. 2007; 25:297–308. [PubMed: 17244536]
27. Hassa PO, Haenni SS, Buerki C, Meier NI, Lane WS, Owen H, Gersbach M, Imhof R, Hottiger MO. Acetylation of poly(ADP-ribose) polymerase-1 by p300/CREB-binding protein regulates coactivation of NF-kappaB-dependent transcription. J Biol Chem. 2005; 280:40450–40464. [PubMed: 16204234]
28. Menard L, Poirier GG. Rapid assay of poly(ADP-ribose) glycohydrolase. Biochem Cell Biol. 1987; 65:668–673. [PubMed: 3325077]
29. Myers JK, Pace CN, Scholtz JM. Helix propensities are identical in proteins and peptides. Biochemistry. 1997; 36:10923–10929. [PubMed: 9283083]
30. Chen YH, Yang JT. A new approach to the calculation of secondary structures of globular proteins by optical rotatory dispersion and circular dichroism. Biochem Biophys Res Commun. 1971; 44:1285–1291. [PubMed: 5168596]
31. Rost B, Yachdav G, Liu J. The PredictProtein server. Nucleic Acids Res. 2004; 32:W321–326. [PubMed: 15215403]
32. Rost B. PHD: predicting one-dimensional protein structure by profile-based neural networks. Methods Enzymol. 1996; 266:525–539. [PubMed: 8743704]
33. Rost B, Sander C. Prediction of protein secondary structure at better than 70% accuracy. J Mol Biol. 1993; 232:584–599. [PubMed: 8345525]
34. Rost B. Review: protein secondary structure prediction continues to rise. J Struct Biol. 2001; 134:204–218. [PubMed: 11551180]
35. Claros MG, Vincens P. Computational method to predict mitochondrially imported proteins and their targeting sequences. Eur J Biochem. 1996; 241:779–786. [PubMed: 8944766]
36. von Heijne G. Mitochondrial targeting sequences may form amphiphilic helices. Embo J. 1986; 5:1335–1342. [PubMed: 3015599]
37. Lemire BD, Fankhauser C, Baker A, Schatz G. The mitochondrial targeting function of randomly generated peptide sequences correlates with predicted helical amphiphilicity. J Biol Chem. 1989; 264:20206–20215. [PubMed: 2555347]
38. Roise D, Theiler F, Horvath SJ, Tomich JM, Richards JH, Allison DS, Schatz G. Amphiphilicity is essential for mitochondrial presequence function. Embo J. 1988; 7:649–653. [PubMed: 3396537]
39. Lithgow T. Targeting of proteins to mitochondria. FEBS Lett. 2000; 476:22–26. [PubMed: 10878243]
40. Koehler CM. Protein translocation pathways of the mitochondrion. FEBS Lett. 2000; 476:27–31. [PubMed: 10878244]
41. Lai Y, Chen Y, Watkins SC, Nathaniel PD, Guo F, Kochanek PM, Jenkins LW, Szabo C, Clark RS. Identification of poly-ADP-ribosylated mitochondrial proteins after traumatic brain injury. J Neurochem. 2008; 104:1700–1711. [PubMed: 17996029]
42. Fong PC, Boss DS, Yap TA, Tutt A, Wu P, Mergui-Roelvink M, Mortimer P, Swaisland H, Lau A, O'Connor MJ, Ashworth A, Carmichael J, Kaye SB, Schellens JH, de Bono JS. Inhibition of poly(ADP-ribose) polymerase in tumors from BRCA mutation carriers. N Engl J Med. 2009; 361:123–134. [PubMed: 19553641]
43. Amir E, Seruga B, Serrano R, Ocana A. Targeting DNA repair in breast cancer: A clinical and translational update. Cancer Treat Rev. (in press).

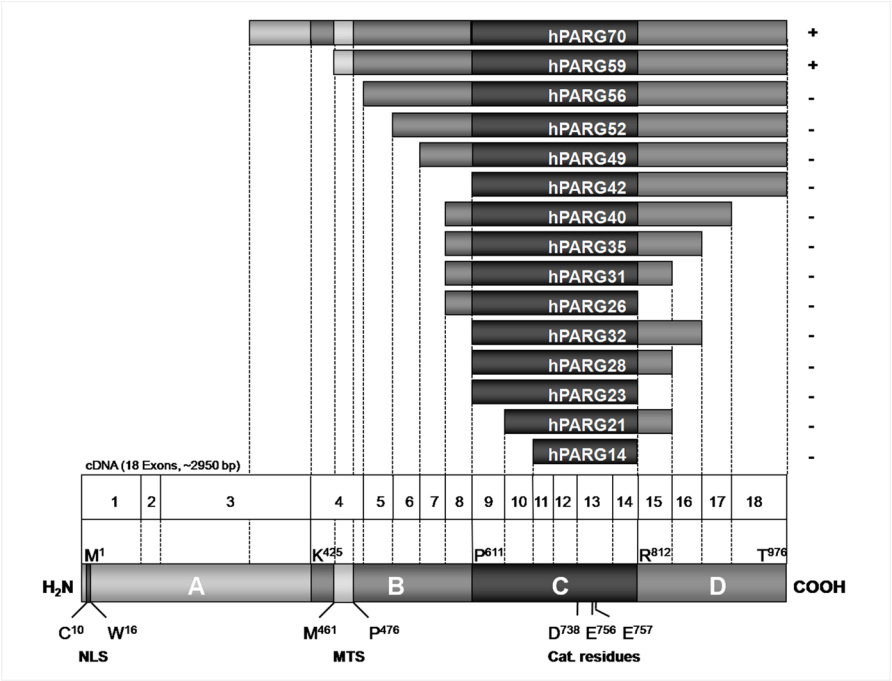

FIGURE 1. Determination of the minimal catalytically active PARG

The fifteen PARG fragments synthesized and tested for enzymatic activity are shown in relation to the full-length hPARG111 protein. Each fragment is labeled according to its size in kilodaltons, and is indicated on the right as being either catalytically active (+) or inactive (−).

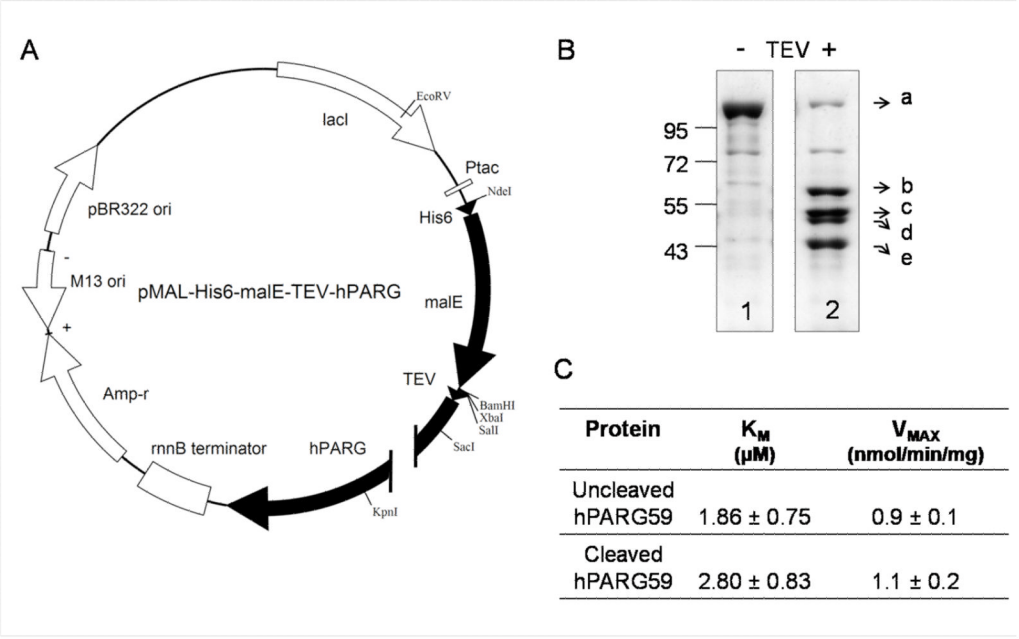

Protein	K_M (μM)	V_{MAX} (nmol/min/mg)
Uncleaved hPARG59	1.86 ± 0.75	0.9 ± 0.1
Cleaved hPARG59	2.80 ± 0.83	1.1 ± 0.2

FIGURE 2. Preparation of PARG fragments and mutants

(A) Bacterial expression plasmid His_6-malE-TEV-hPARG used for the expression of the PARG fragments and mutants discussed in this study. (B) Coomassie blue staining of the Ni^{2+}-purified hPARG59 fragment before (lane 1) and after (lane 2) removal of the His_6-MBP dual tag by TEV. The bands present following cleavage are the uncleaved fusion protein His_6-MBP-TEV-hPARG59 (103 kDa, band a), the cleaved hPARG59 protein (59 kDa, band b), the Pro-TEV protease (50 kDa, band c), the truncated TEV autoproteolysis product (47 kDa, band d) and the cleaved His_6-MBP tag (43 kDa, band e). (C) Enzyme kinetic parameters of bacterially expressed hPARG59 before and after cleavage of the His_6-MBP fusion tag. The K_m and V_{max} values and standard errors were determined using the GraphPad Prism® program, and are expressed as a mean value of a representative experiment carried out in triplicate.

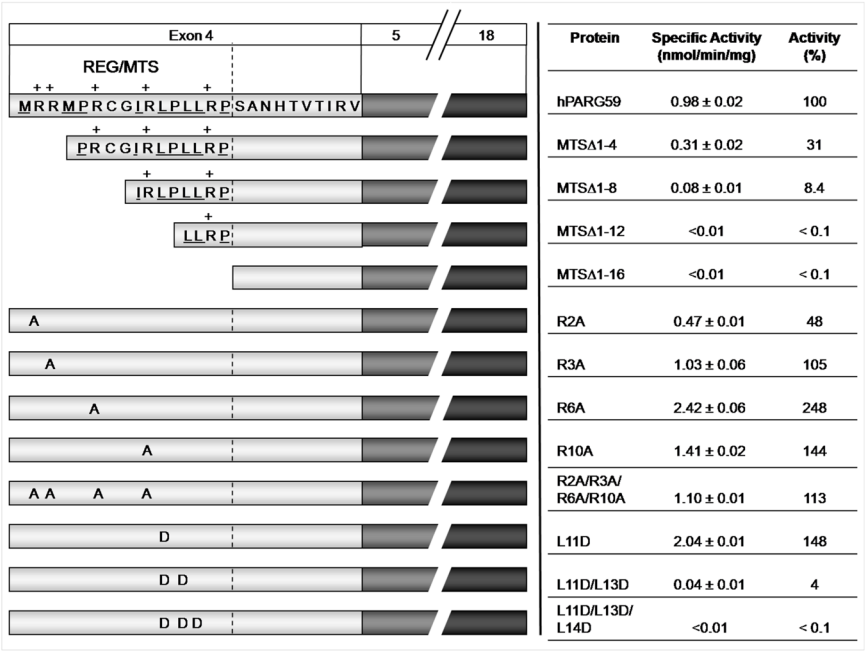

Protein	Specific Activity (nmol/min/mg)	Activity (%)
hPARG59	0.98 ± 0.02	100
MTSΔ1-4	0.31 ± 0.02	31
MTSΔ1-8	0.08 ± 0.01	8.4
MTSΔ1-12	<0.01	< 0.1
MTSΔ1-16	<0.01	< 0.1
R2A	0.47 ± 0.01	48
R3A	1.03 ± 0.06	105
R6A	2.42 ± 0.06	248
R10A	1.41 ± 0.02	144
R2A/R3A/ R6A/R10A	1.10 ± 0.01	113
L11D	2.04 ± 0.01	148
L11D/L13D	0.04 ± 0.01	4
L11D/L13D/ L14D	<0.01	< 0.1

FIGURE 3. Deletion and site-directed mutagenesis of the hPARG59 REG/MTS

The REG/MTS deletion and site-directed mutants are shown in relation to wild-type hPARG59. The exon structure is indicated on the top left. The REG/MTS residues present in each deletion mutant and those mutated by the site-directed mutagenesis are also noted. Basic residues of the REG/MTS are indicated with a plus sign (+) and those that are hydrophobic are underlined. To the right, the specific activity and percent activity of each fragment are listed, with the latter being expressed as a percentage of wild-type hPARG59. Data are shown as means of values from two separate experiments, each performed in triplicate.

A

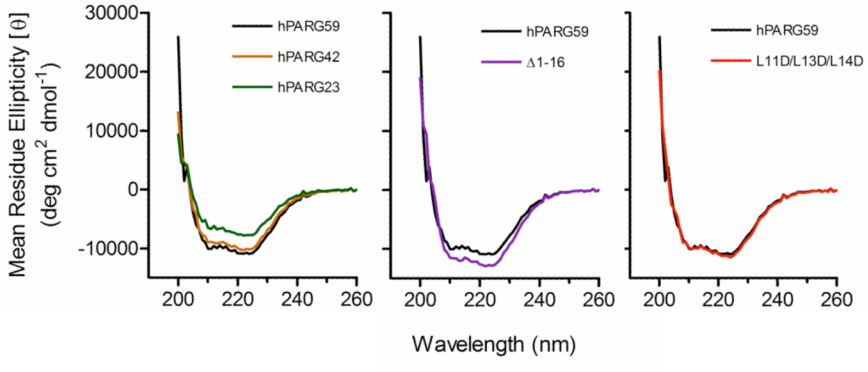

B

Protein	Molecular weight (Daltons)	$[\theta]_{222}$ (deg cm^2 dmol^{-1})	Helicity (%)
hPARG59	102415	-10903	43.7
hPARG42	84941	-10278	41.6
hPARG23	66228	-7833	33.6
Δ1-16	100380	-12943	50.4
L11D/L13D/L14D	102420	-11181	44.6

FIGURE 4. Circular dichroism spectra

(A) The spectra of fragments hPARG42 (brown) and hPARG23 (green), and mutants Δ1-16 (purple) and L11D/L13D/L14D (red) are compared to that of wild type hPARG59 (black). (B) The molecular weight, mean residue ellipticity at 222 nm, $[\theta]_{222}$, and helical fraction of hPARG42, hPARG23, Δ1-16 and L11D/L13D/L14D are compared to those of wild-type hPARG59.

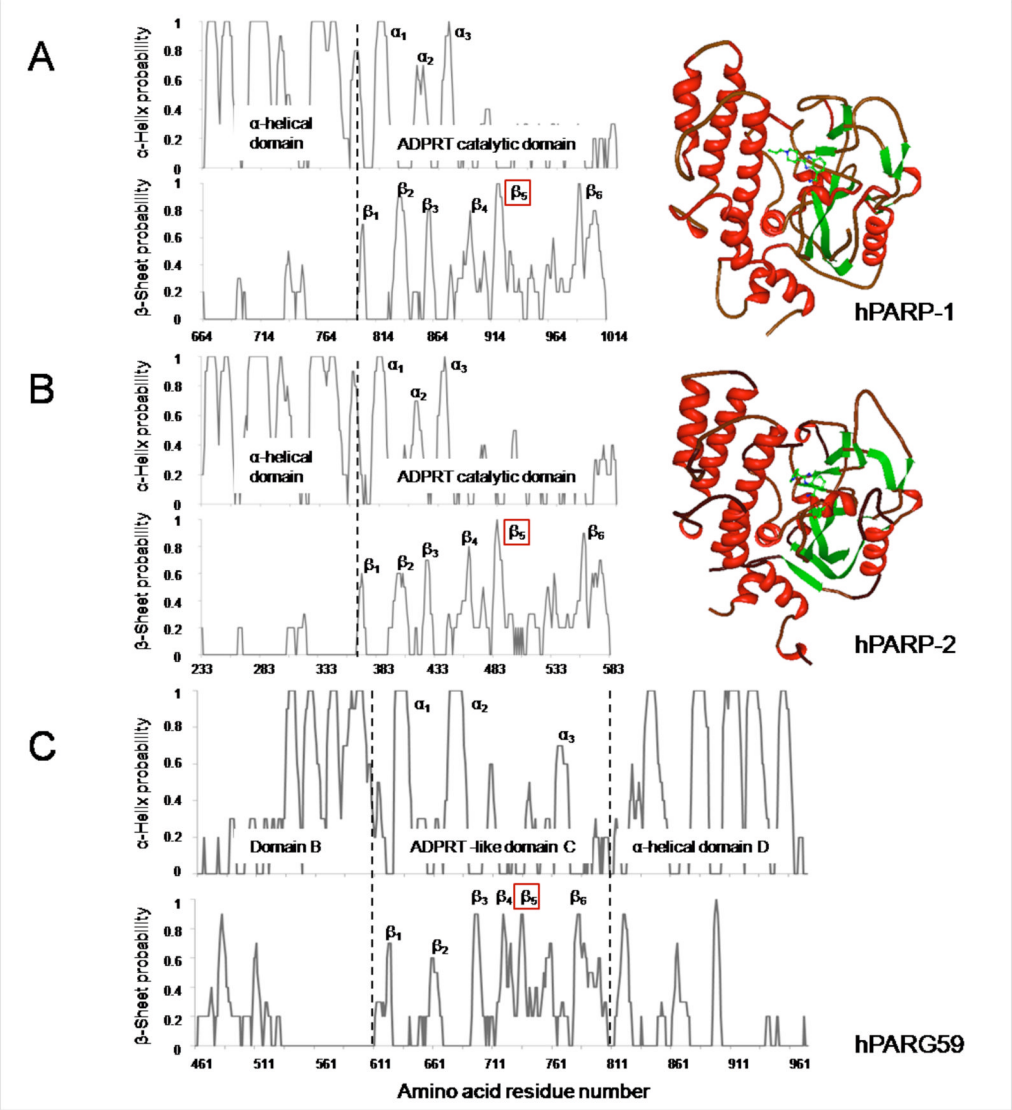

FIGURE 5. Secondary structure predictions

Secondary structure predictions for the mostly α-helical domain and mixed α/β ADPRT catalytic domain of hPARP-1 (A) and hPARP-2 (B) are shown adjacent to their respective crystal structures (Protein Data Bank Identification numbers 2RCW and 3KJD for hPARP-1 and hPARP-2, respectively) and are compared to that of hPARG59 (C). The ADPRT catalytic domain of PARP-1 and PARP-2 and the ADPRT-like catalytic domain C of PARG are aligned to show structural similarity. The α-helices and β-sheets are indicated and β-sheet 5, containing the catalytic glutamate residues of each enzyme, is labeled by a red square. The predictions were carried out using the PHD and $PROF_{sec}$ algorithms as described in Materials and Methods.

A

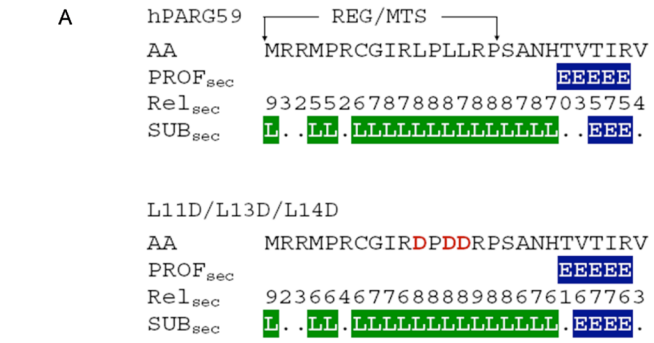

B

Protein	Export to mitochondria probability	Mitochondrial fraction (%)	Cleavage site
hPARG59	0.97	95	P[16]
L11D/L13D/ L14D	0.63	20	ND

FIGURE 6. PARG REG/MTS is predicted to be in a loop conformation

(A) $PROF_{sec}$ secondary structure predictions of the wild-type REG/MTS and L11D/L13D/ L14D mutant. The three mutated residues are shown in red. Abbreviations: AA, amino acid; L, loop; E, β-sheet, Rel_{sec}, reliability index for $PROF_{sec}$ prediction (0 = low to 9 = high); SUB_{sec}, a subset of the $PROF_{sec}$ algorithm for all residues with an expected average accuracy >82 percent. (B) Predicted and observed changes in REG/MTS function induced by the L11D/L13D/L14D mutation. The export to mitochondria probabilities and cleavage site detections were obtained using the MitoProtII computational method (35), while the mitochondrial fraction values have been previously reported (12).

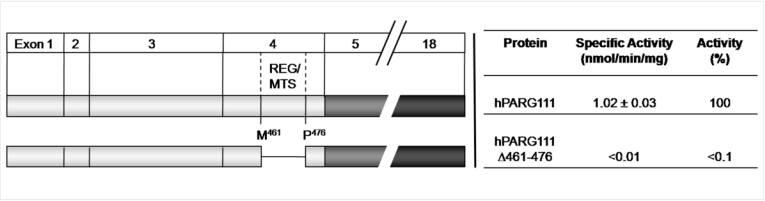

Protein	Specific Activity (nmol/min/mg)	Activity (%)
hPARG111	1.02 ± 0.03	100
hPARG111 Δ461-476	<0.01	<0.1

FIGURE 7. Deletion of the REG/MTS from full-length hPARG111

Deletion mutagenesis was used to characterize the role of the REG/MTS in the enzymatic activity of the full-length hPARG111 protein. The REG/MTS and its first and last amino acid residues are indicated. The specific activities and percent activities are shown as means of values from two separate experiments, each performed in triplicate.

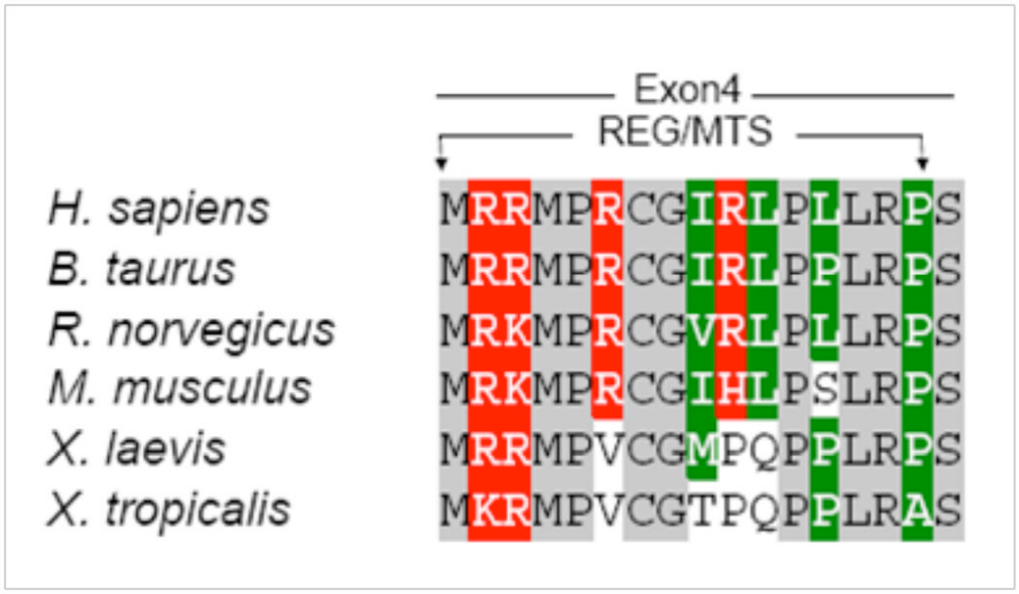

FIGURE 8. Comparison of PARG amino acid sequences from different species

The amino acid sequence of the REG/MTS coded by exon 4 was aligned with five additional PARG sequences across a wide range of organisms. Residues shown in grey represent sequence identity in all six organisms, while those in red and green represent conservation of basic and hydrophobic residues, respectively. The accession numbers for PARG are as follows: Q86W56 for *Homo sapiens*, O02776 for *Bacillus taurus*, Q9QYM2 for *Rattus norvegicus*, O88622 for *Mus musculus*, Q4KLP9 for *Xenopus laevis* and B1H3J2 for *Xenopus tropicalis*.